Correction for Direction-Dependent Distortions in Diffusion Tensor Imaging Using Matched Magnetic Field Maps

Bin Chen, Hua Guo, Allen W. Song
Brain Imaging and Analysis Center, Duke University

Running title: DTI Distortion Correction

Allen W. Song, PhD
Brain Imaging and Analysis Center
Box 3918, DUMC
Duke University
Durham, NC 27710
E-mail: allen.song@duke.edu

Abstract

Diffusion tensor imaging (DTI) has seen increased usage in clinical and basic science research in the past decade. By assessing the water diffusion anisotropy within biological tissues, e.g. brain, researchers can infer different fiber structures important for neural pathways. A typical DTI dataset contains at least one base image and six diffusion weighted images along non-collinear encoding directions. The resultant images can then be combined to derive the three principal axes of the diffusion tensor and their respective cross terms, which can in turn be used to compute fractional anisotropy (FA) maps, apparent diffusion coefficient (ADC) maps, and to construct axonal fibers. The above operations all assume that DTI images along different diffusion-weighting directions for the same brain register to each other without spatial distortions. This assumption is generally false, as the large diffusion-weighting gradients would usually induce eddy currents to generate diffusion-weighting direction dependent field gradients, leading to mis-registration within the DTI dataset. Traditional methods for correcting magnetic field induced distortions do not usually take into account these direction-dependent eddy currents unique for DTI, and they are usually time-consuming because multiple phase images need to be acquired. In this report, we describe our theory and implementation of an efficient and effective method to correct for the main field and eddy current-induced direction-dependent distortions for DTI images under a unified framework to facilitate the daily practice of DTI acquisitions.

Key Words: DTI, Eddy Current, Distortion, Correction, Field Map

Introduction

Magnetic resonance diffusion tensor imaging (DTI) is sensitive to the anisotropic diffusion of water exerted by its macromolecular environment, and has been shown to be useful in characterizing structures of ordered tissues such as the brain white matter and the myocardium (Basser, Mattiello et al. 1994; Mori, Crain et al. 1999). The essence of DTI involves the acquisition of diffusion-weighted images sensitized in various gradient directions. Therefore, a typical DTI experiment requires one base image and at least 6 non-collinear diffusion weighted images. Because of the large datasets, DTI experiments often use fast imaging sequences to reduce the otherwise lengthy acquisition time. However, most fast imaging methods, such as echo-planar imaging (EPI), suffer from image distortions because of the field inhomogeneity (static factor), imperfection of the gradient waveforms, and eddy currents (dynamic factor) during the long readout time. As a result, diffusion weighted images will suffer from both static (due to the main field inhomogeneity) and encoding direction-dependent (due to the diffusion-weighting gradients) distortions. Consequently, the mis-registration among a set of diffusion weighted images will lead to spatial inaccuracies in the derivation of the diffusion tensor, ADC, and FA since they are typically computed on a pixel-by-pixel basis combining all diffusion-weighting directions.

Various methods have been introduced to reduce the distortions caused by the inhomogeneous magnetic field and eddy currents in an EPI image acquisition. For field inhomogeneity correction, one of the most widely used methods is to use a static

magnetic field offset map derived from phase images acquired at two or more different echo times (TEs). After unwrapping and computing the differences among the phase images, the pixel displacement map (mostly along the vulnerable phase-encoding direction) can be inferred from the magnetic field offset map (Jezzard and Balaban 1995). Since the accuracy of the magnetic field offset map relies heavily on the unwrapped phase, many phase unwrapping algorithms have been developed for improved robustness and immunity to noise when the continuous phase evolution information is not available (Cusack, Huntley et al. 1995; Herraez, Gdeisat et al. 2002; Jenkinson 2003). While most 2D or 3D phase unwrapping algorithms unwrap the phase in an image by complex rules, the multi-echo technique (Song 1995; Chen and Wyrwicz 1999; Schmithorst, Dardzinski et al. 2001), as an alternative approach, has been introduced to deliver phase evolution information which leads to highly reliable one-dimensional phase unwrapping. The regression process through the multiple TE images makes the multi-echo method a robust way to accurately compute the field map.

However, eddy currents induced by the diffusion-weighting and EPI imaging gradients, which dynamically influence the global image shape through shearing and scaling, cannot be directly derived from the aforementioned field mapping techniques that only measure and correct the static distortions. In DTI, especially, the diffusion weighted images at different *b* values and encoding directions suffer from direction-dependent geometric distortions due to the direction-dependent eddy currents. That is, each diffusion weighted image within a DTI dataset has its unique geometric distortion. Jezzard et al. introduced an effective method to sample the magnetic field induced by eddy currents in the

frequency and phase directions by interleaved navigated sequences (Jezzard, Barnett et al. 1998). Since two separate measurements are required at the time of each scan, the scan time would be lengthened as a result of collecting the eddy current compensation data. For single shot EPI in particular, the overhead would take two thirds of the scan time. More recently, Andersson et. al. (NeuroImage 20:870-888, 2003) proposed a method to correct EPI image distortion by acquiring two EPI images with opposite phase directions. This retrospective method is an effective technique to register a whole volume and estimate the eddy current at the same time. Nevertheless, their approach requires doubled data acquisition time and increased computational demand for spatial estimation compared to the deterministic fast field map technique. In addition, several other methods have been proposed to estimate the eddy currents through post-processing techniques (Haselgrove and Moore 1996; Bastin 1999; Rohde, Barnett et al. 2004). Although no additional acquisition time is required, it is in general computationally intensive to co-register multiple sets of diffusion weighted images where the contrasts may be highly variable.

Therefore, the goal of geometric distortion correction for DTI images is to correct the distortions caused by a static but subject dependent inhomogeneous field, and a dynamic but subject independent eddy current residual field during data acquisition. While the methods discussed above have been implemented to correct the geometric distortions caused by the field inhomogeneity and eddy currents, a systematic investigation of the correction methodology for diffusion-weighting direction-dependent distortions in DTI acquisition has not been fully carried out. In this report, we propose an integrated

approach to correct the direction-dependent scaling and shearing artifacts caused by eddy current-induced gradient fields, and the non-linear displacement caused by the B_0 field inhomogeneity. It is also inherently deterministic, computationally efficient, and does not require significant additional imaging time.

Methods

To take advantage of the high accuracy of the multi-echo field mapping technique, and to best quantify the magnetic field in the presence of the diffusion-weighting gradients and EPI readout gradients, we have implemented a pulse sequence combining conventional phase encoding steps and EPI readout trains to collect images continuously at progressing echo times to acquire the distortion-free field map (Song 1995) for each diffusion-weighting direction including the base image ($b = 0$). From calibration phase images acquired in a phantom, the field variation maps of the main magnetic field as well as the gradient fields caused by the encoding direction-dependent eddy currents can be computed from the base image and the diffusion weighted images. The field maps can then be used to correct the static and dynamic distortions respectively.

Field map acquisition

The field maps were computed from the images acquired with a blip-less EPI sequence combined with a conventional phase encoding scheme inserted before the EPI readout train (Figure 1). After each excitation, $N \times T$ data points were collected, where N is the

matrix size in the frequency direction and T is the number of TEs. The data can be reorganized into an $N \times N \times T$ volume after N phase encoding steps, and interpreted as a series of $N \times N$ images acquired at consecutive TEs. Each individual image was collected within a very short readout window (< 1 ms) leading to minimal distortions. The phase evolution of a pixel in an $N \times N$ image sampled under a series of TEs was recovered by one-dimensional phase unwrapping (Itoh 1982). The field map ΔB was then calculated from a linear regression between the unwrapped phases Φ and the TEs by the following equation:

$$\Phi_i = \Phi_0 + \gamma \Delta B * TE_i, \quad i = 1,2...T \qquad [1]$$

where Φ_i is the unwrapped phase, Φ_0 is a constant, and γ is the gyromagnetic ratio. For improved accuracy, the odd and even images, which correspond to the forward and backward readout directions, were fitted separately to remove the influence of off-resonance effects or constant background fields. The resulting ΔB was then derived as the average of the odd and even field maps. In the images acquired for this report, N and T were both set to 64. However, depending upon the desired spatial resolution for DTI, a different [N, T] combination could be used. For example, at a higher spatial resolution of 128 × 128, one could use a combination of [128, 32] to reduce the length of EPI readout train to keep the same TR or to accommodate more slices.

Phantom images were acquired at TE of 100 ms and TR of 800 ms with an isopropyl alcohol phantom, whose diffusivity is close to the diffusivity of the human brain. The human data were collected with the same TE and TR. The same FOV of 32 cm was used. Both sets of data were acquired after standard whole-volume automatic high order

shimming (typically 5 Hz rms for phantom and 20 Hz rms for human). The long TE was used to accommodate the diffusion-weighting gradients, which were the same in each diffusion direction for both field mapping unit and DTI imaging sequences.

All sequence development and data acquisition were conducted on a whole-body 4T GE Signa Horizon LX system (GEMS, Milwaukee, Wisconsin), under the approval of the Institutional Review Board of the Duke University.

ΔB_0 and eddy current-induced field gradient (G') calibration

While the inhomogeneous field is the main reason for the base image distortion, the distortion of the diffusion weighted images results from the combination of the inhomogeneous field (which is the same for the base image) and eddy currents from strong diffusion gradients. Therefore, the gradient errors due to eddy currents for each diffusion weighted image can be computed by taking the gradient of the difference map between the field map of the diffusion weighted image and the field map of the base image:

$$\begin{aligned} G'_{x,i} &= \frac{\partial}{\partial x}(\Delta B_i - \Delta B_0) \\ G'_{y,i} &= \frac{\partial}{\partial y}(\Delta B_i - \Delta B_0) \\ G'_{z,i} &= \frac{\partial}{\partial z}(\Delta B_i - \Delta B_0) \end{aligned} \qquad [2]$$

where ΔB_0 is the field map of the base image, ΔB_i (i = 1,2…6) is the field map under diffusion-weighting along a given direction, and [$G'_{x,i}, G'_{y,i}, G'_{z,i}$] are eddy current-induced

gradients in the frequency encoding, phase encoding and slice-selective directions respectively for that given diffusion-weighting direction. In this report, six non-collinear directions were used, which resulted in six sets of $[G'_{x,i}, G'_{y,i}, G'_{z,i}]$ maps. In general, eddy current-induced field gradients in the frequency and phase encoding directions would lead to k-space shearing and scaling (e.g. stretching or compressing) effects respectively (Jezzard, Barnett et al. 1998). The small eddy current-induced field gradient in the slice-selective direction may cause signal loss (the induced z-gradient), and image shift and ghosting (the B_0 offset and its effect on odd and even lines of EPI images) in our implementation. While the signal loss does not lead to geometric distortion, the ghosting effect causes a Nyquist ghost along the phase direction. In our experiments, the signal losses were consistently on the order of 1.5% when the diffusion gradient was in the slice direction. The ghosting artifact was effectively eliminated during the reconstruction process since our pulse sequence has an internal reference line in the center of k-space for even and odd lines to account for any potential offsets. As a result, our images do not have observable image shift or ghosting artifact. Because these small eddy currents in the slice-selective direction are not the source of noticeable signal loss and geometric distortion in diffusion weighted images, the computation of G'_z was not emphasized in this report.

In theory, the eddy current is fully determined by the diffusion gradient pulse amplitude, separation and shape; thus, the eddy current decay is a deterministic process when the diffusion gradients are given. The magnitudes of the eddy current-induced field errors are the same at a certain time point, regardless of the scanning objects (e.g. phantom or

human brain). This hypothesis was further confirmed by experiments in phantoms and human in our results. Therefore, in practice, the quantification of the eddy current-induced field gradient can be performed in a phantom on a less frequent basis (e.g. monthly) and applied to human images for distortion correction, provided that identical diffusion-weighting gradients are used in both experiments. The time needed for this one-time procedure is usually dependent on the number of diffusion encoding directions, typically on the order of ten minutes over the entire brain volume for a set of six encoding directions. On the other hand, the static field offset map ΔB_0 needs to be acquired on each individual subject, and usually takes less time to complete. For example, at a TR of 1.5 s which can usually accommodate multiple slices to cover the entire brain, the extra scan time for the ΔB_0 map is less than two minutes. Such a time penalty can be well tolerated by clinical and basic science experiments.

Distortion Estimation and Correction

Under our experimental condition, a magnetic field with a ¼ ppm offset will correspond to approximately a two pixel shift in the phase direction for a 64 × 64 image with the 125 kHz data acquisition bandwidth on our 4T scanner. Eddy current-induced gradients on the order of 0.1% of the readout gradient will cause more than two pixels in shearing and scaling effects at the edges of a 64 × 64 image. Both shearing and scaling have effects in the phase-encoding direction of an image.

Once the eddy current-induced gradients of the DTI acquisition are known after the calibration procedure, the magnitudes of shearing and scaling in a diffusion-weighed image can be derived from the eddy current-induced gradients in the frequency and phase directions respectively. Usually the shearing and scaling effect in terms of pixel shifts in the images can be corrected by the standard affine transformation. However, in this study, the implementation of distortion correction warps the image in one step based on a new field map formed by combining the ΔB_0 field map and eddy current-induced gradient field maps. The intensity value of each pixel in the corrected image is linearly interpolated from the distorted image at the shifted location. This integrated approach minimizes the image blurring effect often seen in the affine transformation. After a combined correction for distortions caused by the inhomogeneous field and eddy currents, the entire diffusion weighted image set can then be considered distortion-free and well registered for further DTI calculations such as the derivation of FA, ADC and fiber tracts.

Results

For the phantom calibration, seven field maps were calculated under a full set of diffusion-weighting gradients including the baseline condition (Figure 2). The eddy current-induced residual fields (Figure 3) computed by removing the ΔB_0 component were used to derive the gradient fields $[G_x', G_y', G_z']$ for different diffusion-weighting directions. The measured residual fields along the frequency and phase encoding directions for all six diffusion-weighting conditions are shown in Figure 4a and 4b, respectively. It can be seen that the eddy current-induced gradient fields, whether along

the principal axes or orthogonal directions due to gradient cross terms, can indeed be modeled as linear. The computed eddy current-induced gradients are listed in Table 1. This small eddy current-induced gradient field, which corresponds to approximately 0.025% of the readout gradient amplitude, would cause shearing and scaling effects that result in more than one pixel displacement along the phase direction across the image.

Table 1: Eddy current gradients in the frequency and phase directions and the induced shearing and scaling values in pixels across the image

DWI	Diffusion Scheme			Frequency	Phase	Shear	Scale
	Gx	Gy	Gz	(10^{-3} gauss/cm)	(10^{-3} gauss/cm)	(pixels)	(pixels)
b1	1	0	0	-0.23	-0.10	-1.38	-0.59
b2	0	1	0	0.06	-0.28	0.38	-1.73
b3	0	0	1	-0.03	0.02	-0.17	0.09
b4	0.7	0.7	0	-0.08	-0.24	-0.51	-1.45
b5	0	0.7	0.7	0.07	-0.19	0.42	-1.17
b6	0.7	0	0.7	-0.14	-0.06	-0.88	-0.37

* Negative value indicates counter-clockwise shear or compression of the image, positive value indicates clockwise shear or stretching of the image.

To better illustrate the effects of ΔB_0 and eddy currents, a set of DTI images (baseline + six directions) without any correction are shown in Figure 5, along with those with ΔB_0 correction in Figure 6, and those with ΔB_0 and eddy current corrections in Figure 7.

While ΔB_0 corrected most of the static distortions (Figure 6), the eddy current-induced shearing and scaling effects can only be removed with a full correction (Figure 7). To better illustrate the direction-dependent eddy current effect, the difference images between Figure 6 and Figure 7 are shown in Figure 8. It is evident that a diagonal shear is prominent in images when the x-diffusion gradient is turned on (e.g. Gx, GxGy, GxGz), while a stretching effect is more visible when the y-diffusion gradient is present (e.g. Gy, GxGy, GyGz). When the z-diffusion gradient is on, the induced eddy current may cause signal loss (the induced z-gradient) and image shift and ghosting (the B_0 offset and its effect on odd and even lines of EPI images). In our data, the signal loss was consistently on the order of 1.5%, which would not lead to significant error in ADC and FA estimation and hence was neglected. The image shift and ghosting artifact were effectively eliminated during the reconstruction process, as our pulse sequence has an internal reference line in the center of k-space for even and odd lines to correct for any drift and offset. As a result, our images did not have observable image shift or ghosting artifact.

In principle, the eddy current-induced gradient fields can be well characterized just once on the phantom for a particular DTI pulse sequence, such that a field map of the base image without diffusion-weighting (i.e. ΔB_0) is the only one that needs to be collected during a DTI experiment in humans. In this report, ΔB_0 and the DTI eddy current-induced gradient fields were all collected in human brains to assess the consistency of the eddy current-induced gradient field correction. The eddy current-induced gradients were also computed from the human dataset to verify their subject-independent property. It

was found that the eddy current-induced gradient in the frequency direction was -0.21×10^{-3} gauss/cm when Gx was on, and that in the phase direction was -0.29×10^{-3} gauss/cm when Gy was on. These results are highly comparable to the phantom results which were -0.23×10^{-3} gauss/cm in the frequency direction and -0.28×10^{-3} gauss/cm in the phase direction, establishing the basis for using the field maps obtained from the phantom to correct the distorted brain images. The eddy current when Gz was turned on induced signal loss on the same order of ~1.5% as the phantoms and caused no ghosting artifact with our reconstruction algorithm incorporating the internal reference line. Its effect was thus not emphasized in this report. We believe this reproducibility of eddy current-induced gradients supports the notion of the subject-independent character of eddy currents since the eddy currents are fully determined by specific diffusion-weighting gradient pulses.

Figure 9 shows a typical set of human DTI images (base + six diffusion-weighting directions) along with those after only ΔB_0 correction, shown in Figure 10. The full correction results were virtually identical using the eddy current-induced gradient field maps derived from either the human brain or the phantom. Shown in Fig. 11 are the final images after a full correction using the brain ΔB_0 map and the eddy current gradient field maps derived from the phantom. While the static distortion in areas such as in the frontal lobe is largely warped back to its original spatial location after ΔB_0 correction, the eddy current-induced shearing and scaling effects can only be removed with a full correction. The difference images between ΔB_0 and full corrections are shown in Figure 12, which have the same spatial and intensity characteristics as the phantom images shown in

Figure 8 and Table 1, demonstrating a high consistency of the eddy current-induced gradient field correction.

Discussion

One clear advantage of the proposed field mapping technique is that the phase can be accurately unwrapped along the continuously sampled TEs on a pixel-by-pixel basis with a 1D unwrapping algorithm. It is more suitable than 2D or 3D phase unwrapping algorithms under the condition of relatively low resolution and larger slice thickness. The field map calculation heavily relies on the accuracy of phase unwrapping. The reliably unwrapped phase information in the multi-echo acquisition can increase the robustness of the distortion-free field map computation.

Another advantage of the current method is its high acquisition speed resulting from the EPI readout train. As such, this approach is practical for daily use. Even with both the eddy current gradients and ΔB_0 maps acquired, the entire procedure can typically be accomplished within minutes. Further, eddy current calibration does not need to be performed on a subject-by-subject basis if the same DTI pulse sequence is used for all experiments; rather, it can be collected once on a uniform phantom (with a slightly larger dimension than the brain to be inclusive) and applied across all subjects, as demonstrated in the results. The ΔB_0 map, however, should be run on a subject-by-subject basis, which would typically take less than two minutes to cover the entire brain. In our implementation, the separated regression procedure for the positive and negative readout

gradients can account for the off-resonance effects potentially present during imaging and the timing delays between the onset of data acquisition and readout gradient. Consequently, this new method can offer accurate, efficient, and matched magnetic field maps to correct for the direction-dependent DTI distortions.

Incidentally, the necessity for field mapping correction is further increased for higher resolution scans, such as 128 and 256 matrices. The time needed for acquiring the field maps are not necessarily increased since a reduced number of echoes during the EPI readout train could be acquired, resulting in a shorter TR or accommodating more slices within the same TR. For example, an accurate field map could be achieved with 32 echoes for an image with the 128 or 256 matrix size. More recently, the use of sensitivity-encoded (SENSE) acquisitions, although reducing the data acquisition window length, would still leave significant distortions as the readout duration would still be in the tens of millisecond range. Efforts are currently underway to incorporate our correction methodology into a SENSE acquisition scheme.

Conclusion

We have demonstrated an efficient and effective method that integrates the field inhomogeneity and eddy current corrections within the same general framework. Its ability in correcting the diffusion weighting-direction dependent distortions unique in the DTI acquisition allows much improved co-registration within the DTI dataset and will

facilitate the increased utilization of DTI techniques in basic and clinical neuroscience research.

Acknowledgements

This work was supported by research grants RR 21382, NS 41328, and NS 50329 from the National Center of Research Resources and National Institute of Neurological Disorders and Stroke at the National Institutes of Health. The authors would like to thank Drs. Todd B. Harshbarger and Trong-Kha Truong in our laboratory for helpful discussions and the two anonymous reviewers for their valuable comments.

References

Andersson, J. L., Skare S., Ashburner, J., 2003. How to correct susceptibility distortions in spin-echo echo-planar images: application to diffusion tensor imaging. Neuroimage 20(2): 870-88.

Basser, P. J., Mattiello J., LeBihan, D., 1994. MR diffusion tensor spectroscopy and imaging. Biophys J 66(1): 259-67.

Bastin, M. E., 1999. Correction of eddy current-induced artefacts in diffusion tensor imaging using iterative cross-correlation. Magn Reson Imaging 17(7): 1011-24.

Chen, N. K. and Wyrwicz, A. M., 1999. Correction for EPI distortions using multi-echo gradient-echo imaging. Magn Reson Med 41(6): 1206-13.

Cusack, R., Huntley, J., Goldrein, H. T., 1995. Improved Noise-Immune Phase-Unwrapping Algorithm. Appl Opt 34(5): 781-789.

Haselgrove, J. C. and Moore, J. R., 1996. Correction for distortion of echo-planar images used to calculate the apparent diffusion coefficient. Magn Reson Med 36(6): 960-4.

Herraez, M. A., Gdeisat, M. A., Burton, D. R. Lalor, M. J., 2002. Robust, fast, and effective two-dimensional automatic phase unwrapping algorithm based on image decomposition. Appl Opt 41(35): 7445-55.

Itoh, K., 1982. Analysis of the phase unwrapping algorithm. Appl Opt 21(14): 2470.

Jenkinson, M., 2003. Fast, automated, N-dimensional phase-unwrapping algorithm. Magn Reson Med 49(1): 193-7.

Jezzard, P. and Balaban, R. S., 1995. Correction for geometric distortion in echo planar images from B0 field variations. Magn Reson Med 34(1): 65-73.

Jezzard, P., Barnett A. S., Pierpaoli, C., 1998. Characterization of and correction for eddy current artifacts in echo planar diffusion imaging. Magn Reson Med 39(5): 801-12.

Mori, S., Crain, B. J., Chacko, V. P., van Zijl, P. C., 1999. Three-dimensional tracking of axonal projections in the brain by magnetic resonance imaging. Ann Neurol 45(2): 265-9.

Rohde, G. K., Barnett, A. S., Basser, P. J., Marenco, S., Pierpaoli, C., 2004. Comprehensive approach for correction of motion and distortion in diffusion-weighted MRI. Magn Reson Med 51(1): 103-14.

Schmithorst, V. J., Dardzinski, B. J., Holland, S. K., 2001. Simultaneous correction of ghost and geometric distortion artifacts in EPI using a multiecho reference scan. IEEE Trans Med Imaging 20(6): 535-9.

Song, A. W., Wang, Y., Tan, S. G., Hyde, J. S., Li, S-J., 1995. Measurement of T2* Value Using Phase Encoded EPI. Proc. SMR, 669.

Figure Legends

Figure 1: Schematic illustration of the pulse sequence for acquiring the matched field maps for the base and diffusion weighted images to determine the static field map and eddy current-induced gradient fields.

Figure 2: Field maps of the base image and six diffusion weighted images.

Figure 3: Residual fields caused by eddy currents.

Figure 4: The eddy current-induced residual fields along arbitrarily selected lines (illustrated in Figure 3) in the frequency-encoding (horizontal) direction (4a) and phase-encoding (vertical) direction (4b). Dominant linear components of the eddy current-induced fields are shown along the frequency-encoding direction when Gx gradient is present and along the phase-encoding direction when Gy is present, and weaker linear components are shown along orthogonal directions due to gradient cross-terms. Eddy current induced by Gz gradient usually induces frequency offset.

Figure 5: DTI dataset of the isopropyl alcohol phantom containing one base image and six diffusion weighted images.

Figure 6: Phantom DTI dataset after geometric correction using ΔB_0 field map only.

Figure 7: Phantom DTI dataset after full correction procedure using ΔB_0 and eddy current field maps.

Figure 8: The difference images between Figure 7 (full correction) and Figure 6 (ΔB_0 correction only). The corresponding shearing and scaling effects due to eddy currents are indicated by arrows.

Figure 9: Human DTI dataset containing one base image and six diffusion weighted images, along with the ΔB_0 map which is always required for each subject.

Figure 10: Human DTI dataset after geometric correction using brain ΔB_0 field map only.

Figure 11: Human DTI dataset after the full correction procedure using the brain ΔB_0 field map and eddy current gradient field maps derived from the phantom.

Figure 12: The difference images between Figure 11 (full correction) and Figure 10 (ΔB_0 correction only). The corresponding shearing and scaling effects due to eddy currents are indicated by arrows, which are highly consistent with those in Figure 8.

Table

Table 1: Eddy current gradients in the frequency and phase directions and the induced shearing and scaling values in pixels across the image

DWI	Diffusion Scheme			Frequency (10^{-3} gauss/cm)	Phase (10^{-3} gauss/cm)	Shear (pixels)	Scale (pixels)
	Gx	Gy	Gz				
b1	1	0	0	-0.23	-0.10	-1.38	-0.59
b2	0	1	0	0.06	-0.28	0.38	-1.73
b3	0	0	1	-0.03	0.02	-0.17	0.09
b4	0.7	0.7	0	-0.08	-0.24	-0.51	-1.45
b5	0	0.7	0.7	0.07	-0.19	0.42	-1.17
b6	0.7	0	0.7	-0.14	-0.06	-0.88	-0.37

* Negative value indicates counter-clockwise shear or compression of the image, positive value indicates clockwise shear or stretching of the image.

Figure1

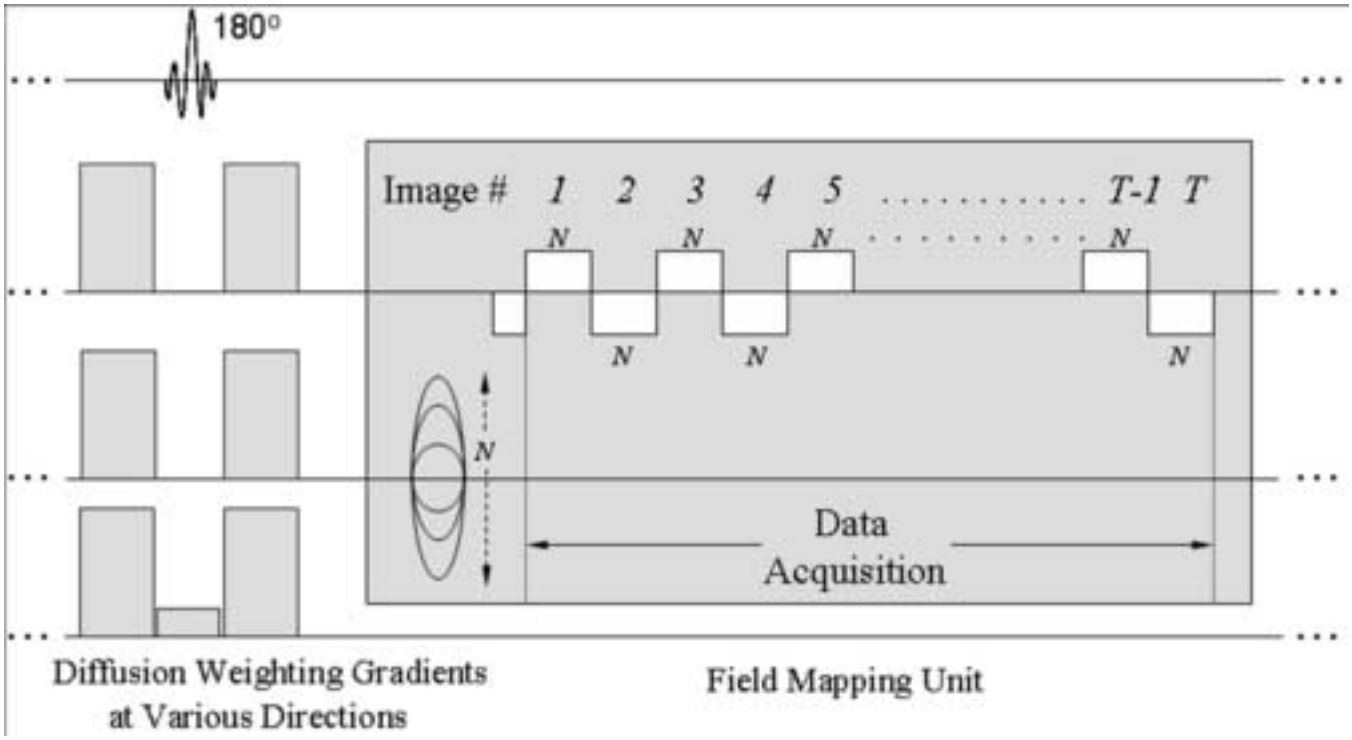
180°
Image # 1 2 3 4 5 ..... T-1 T
N
Data
Acquisition
Diffusion Weighting Gradients
at Various Directions
Field Mapping Unit

Figure2

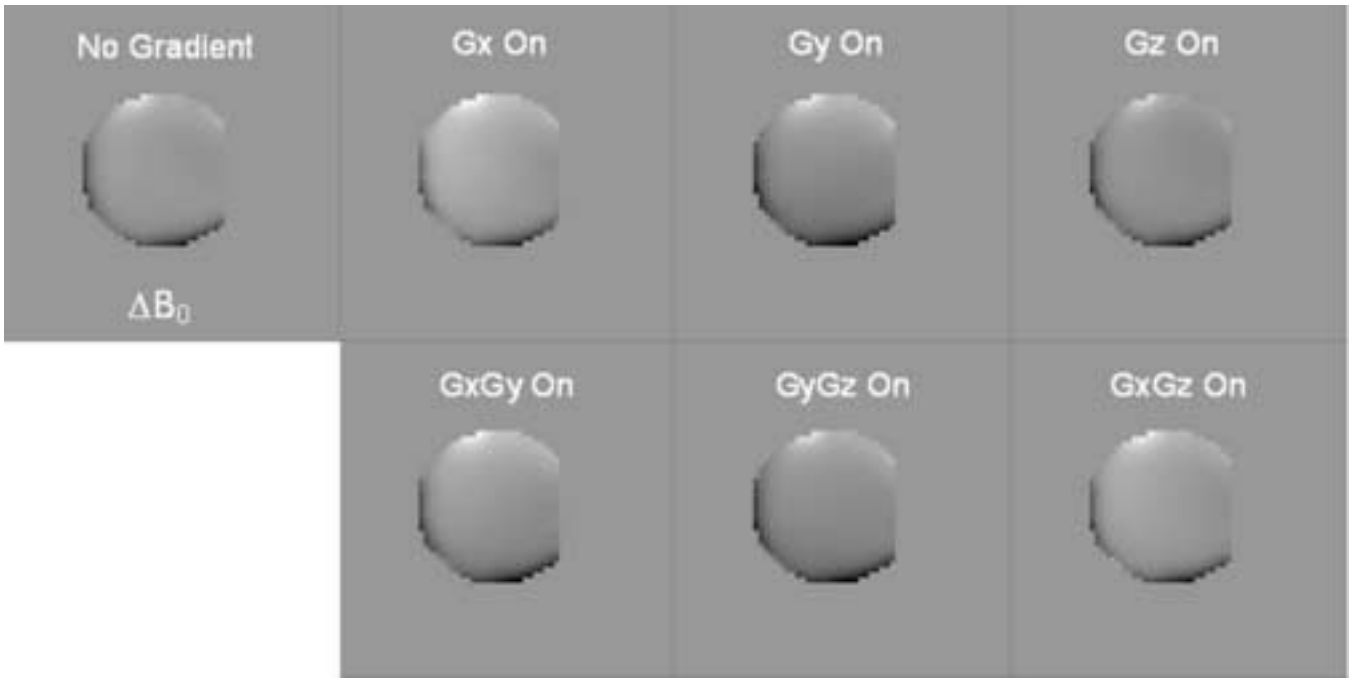

Figure3

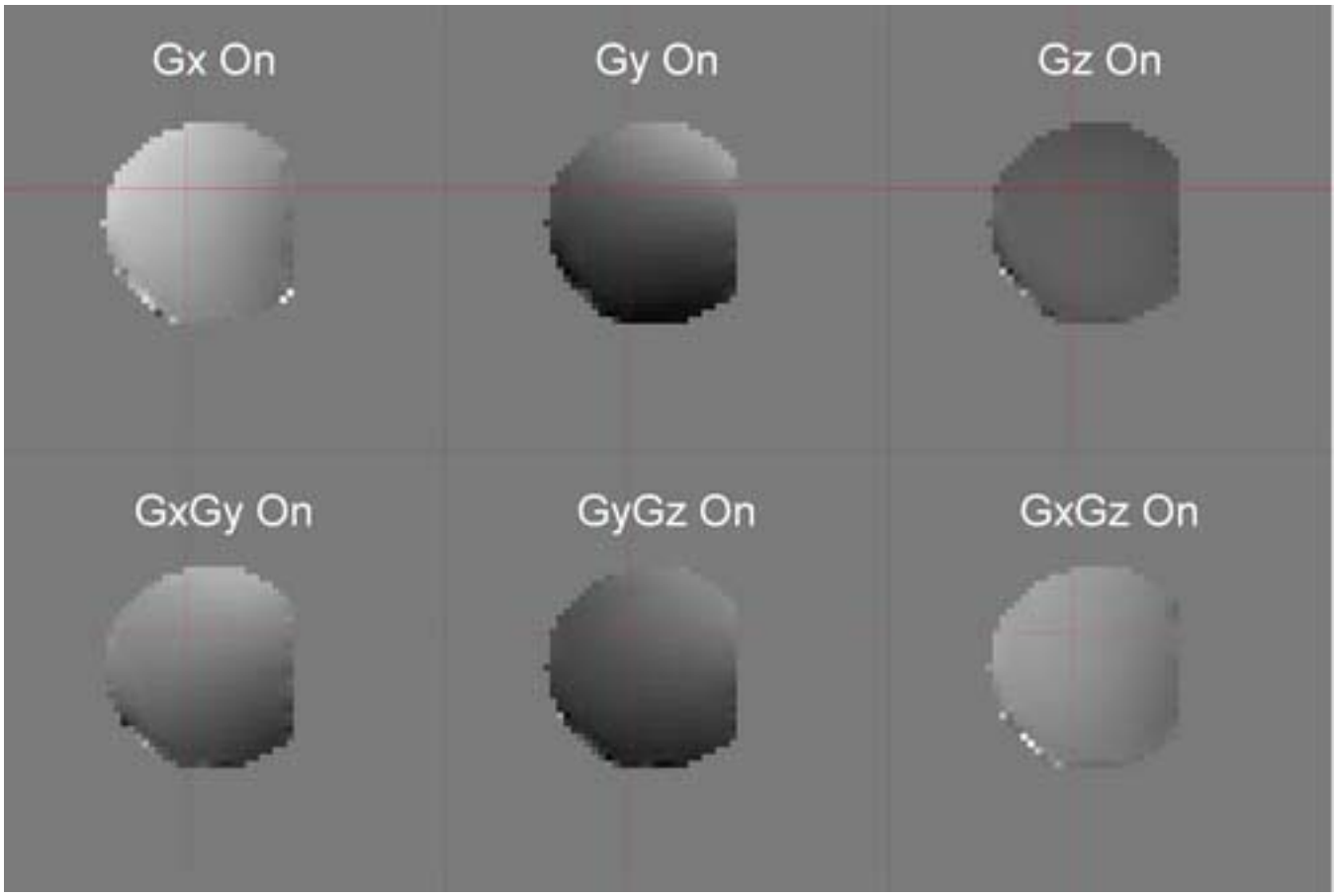

Figure4a

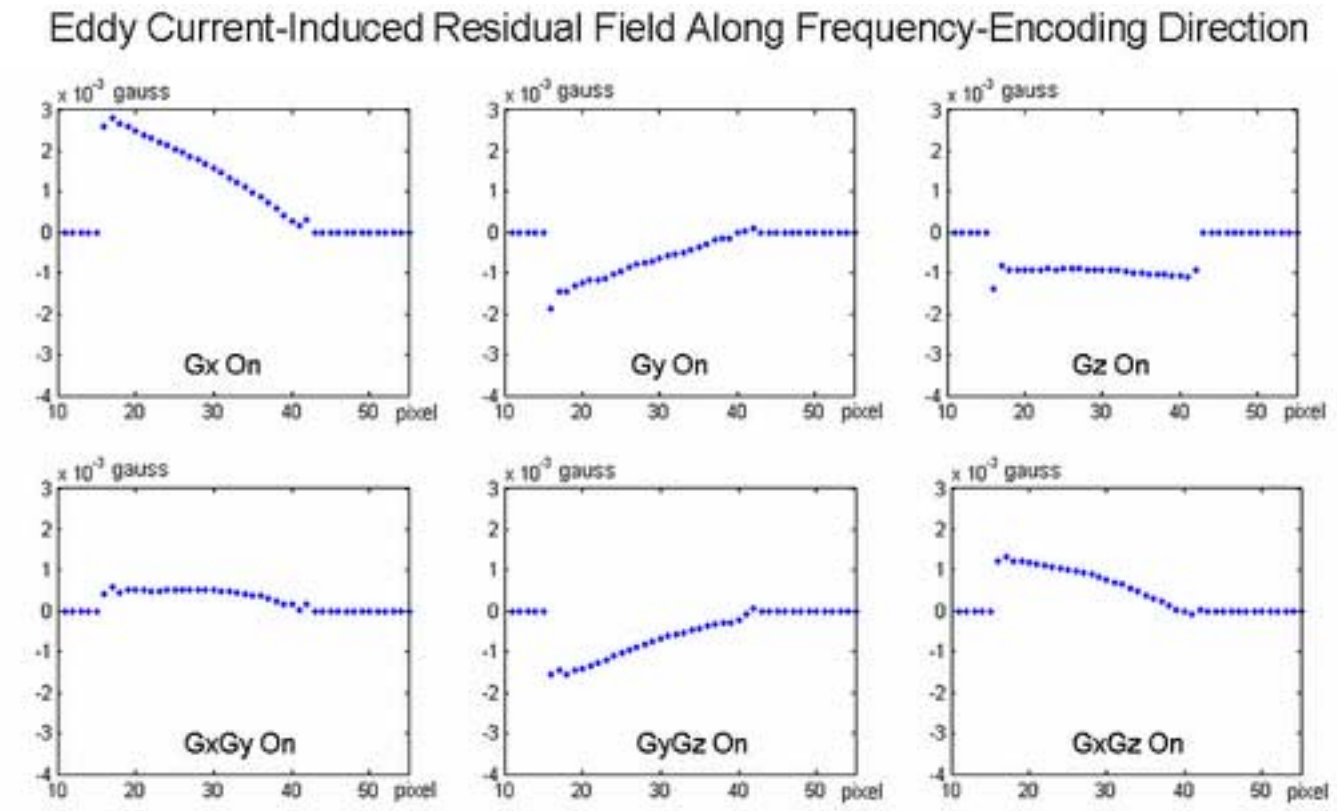
Eddy Current-Induced Residual Field Along Frequency-Encoding Direction
x 10^-3 gauss
Gx On
Gy On
Gz On
GxGy On
GyGz On
GxGz On
pixel

Figure4b

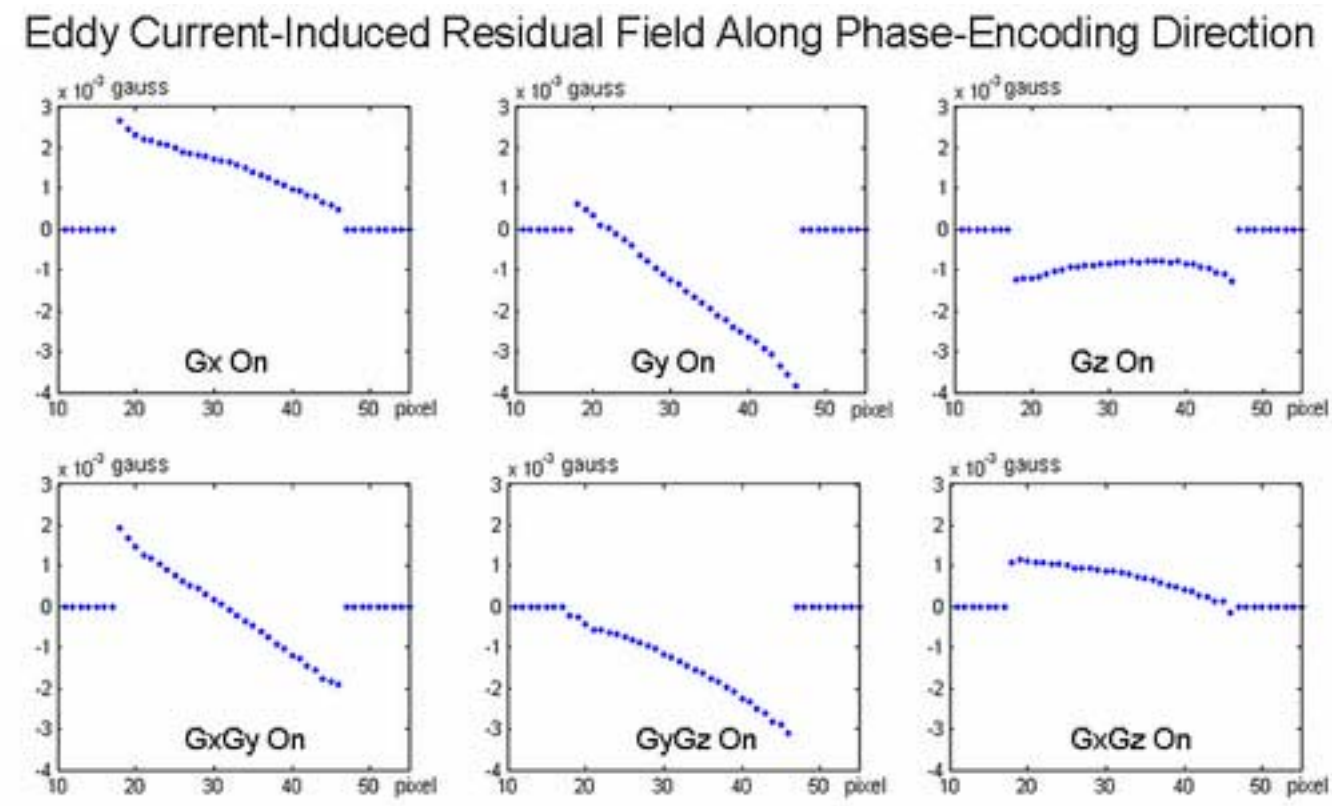
Eddy Current-Induced Residual Field Along Phase-Encoding Direction
x 10^-3 gauss
Gx On
Gy On
Gz On
GxGy On
GyGz On
GxGz On
pixel

Figure5

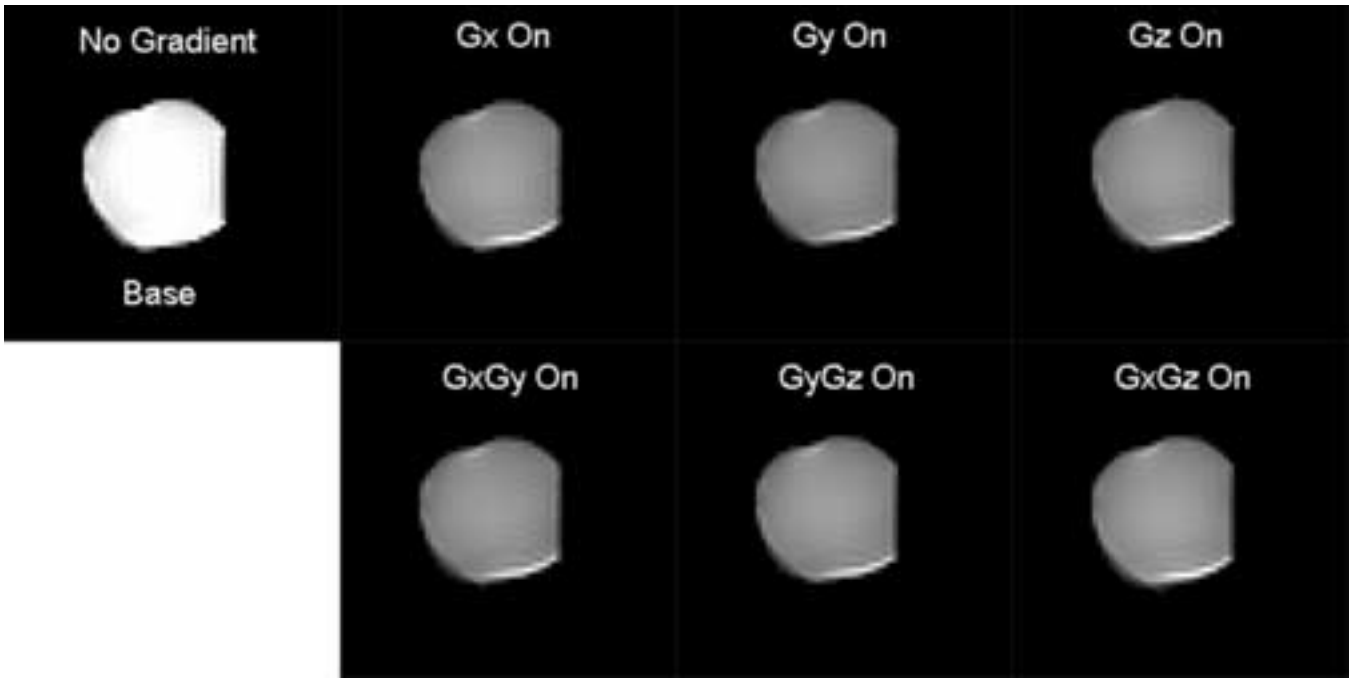

Figure6

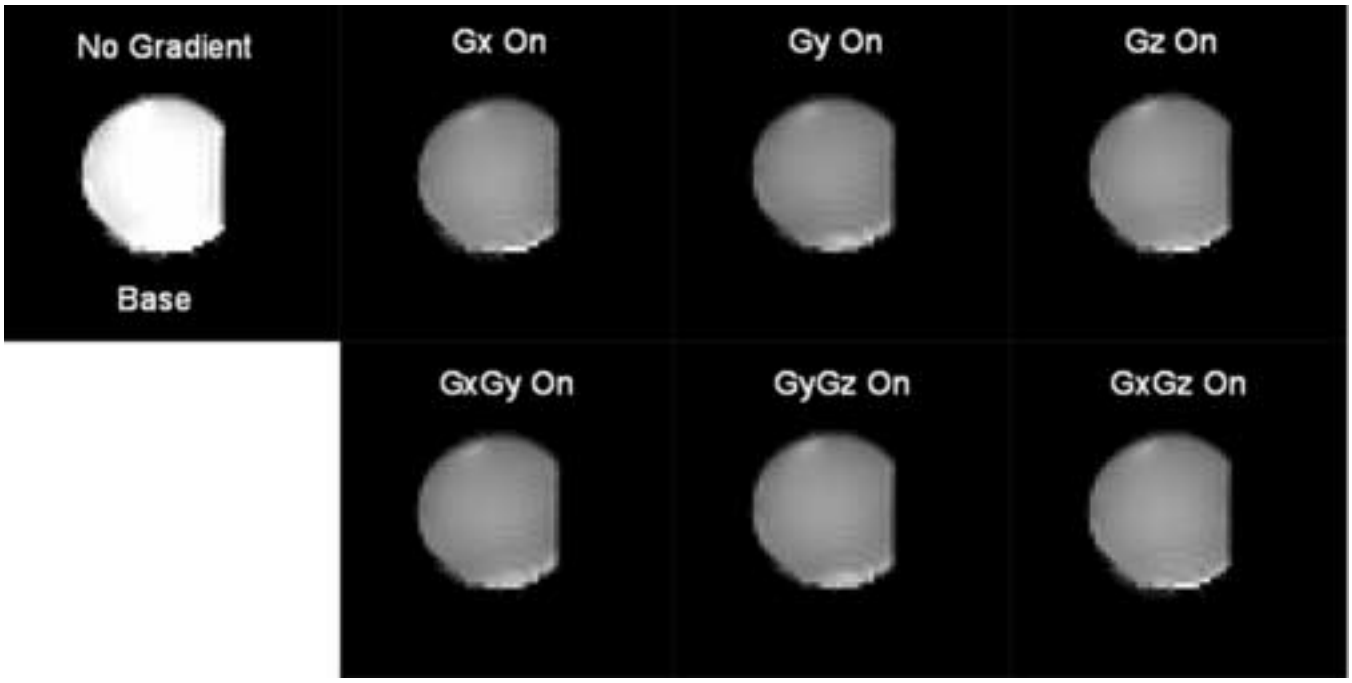

Figure7

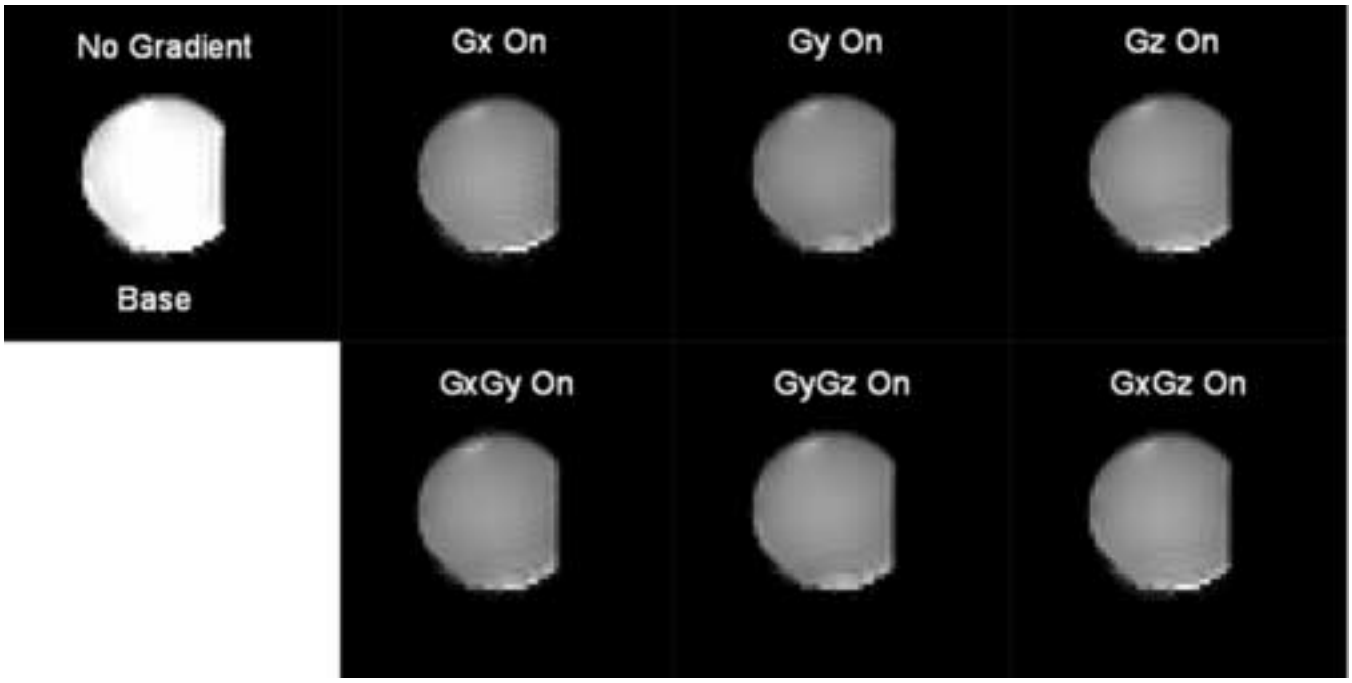

Figure8

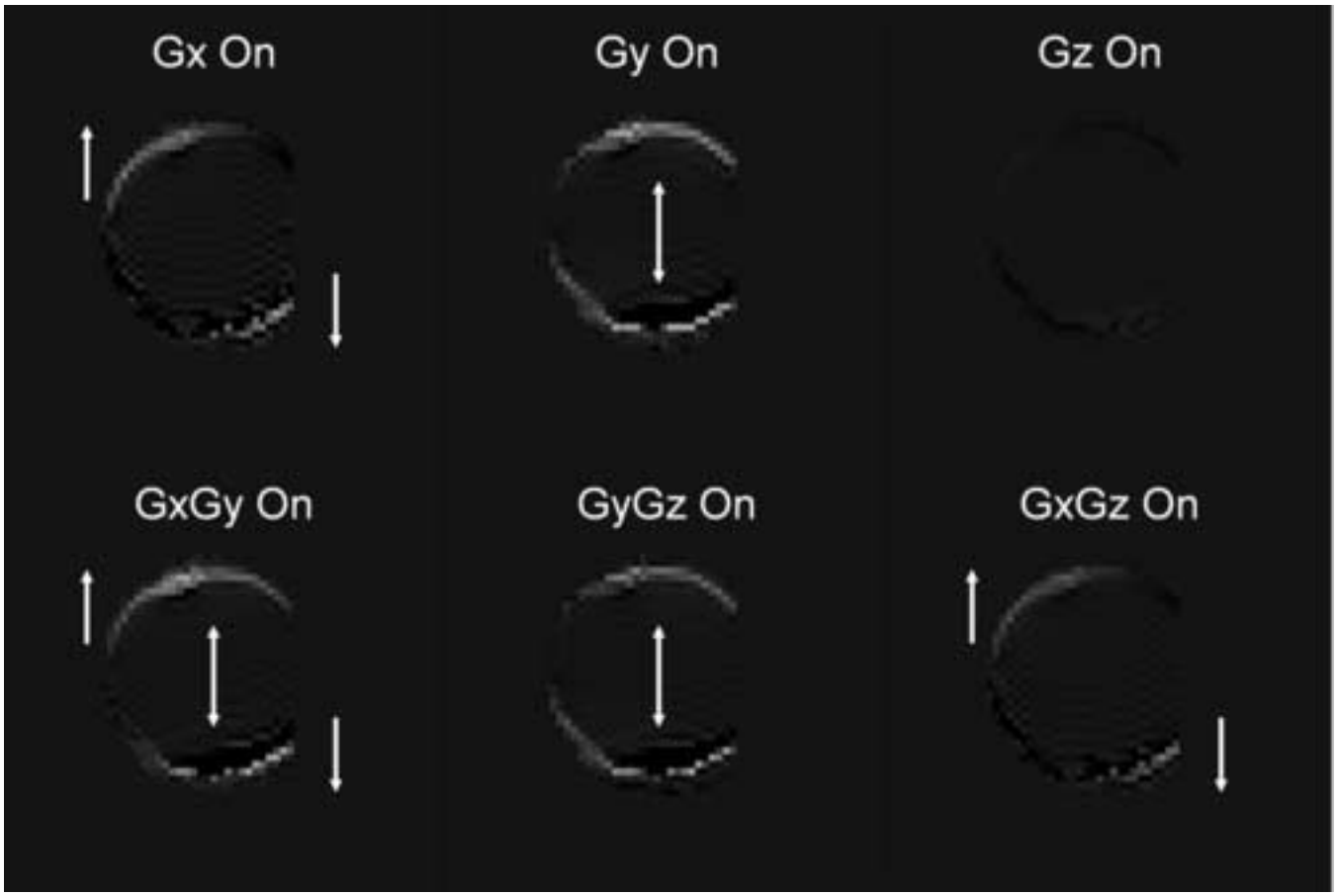

Figure9

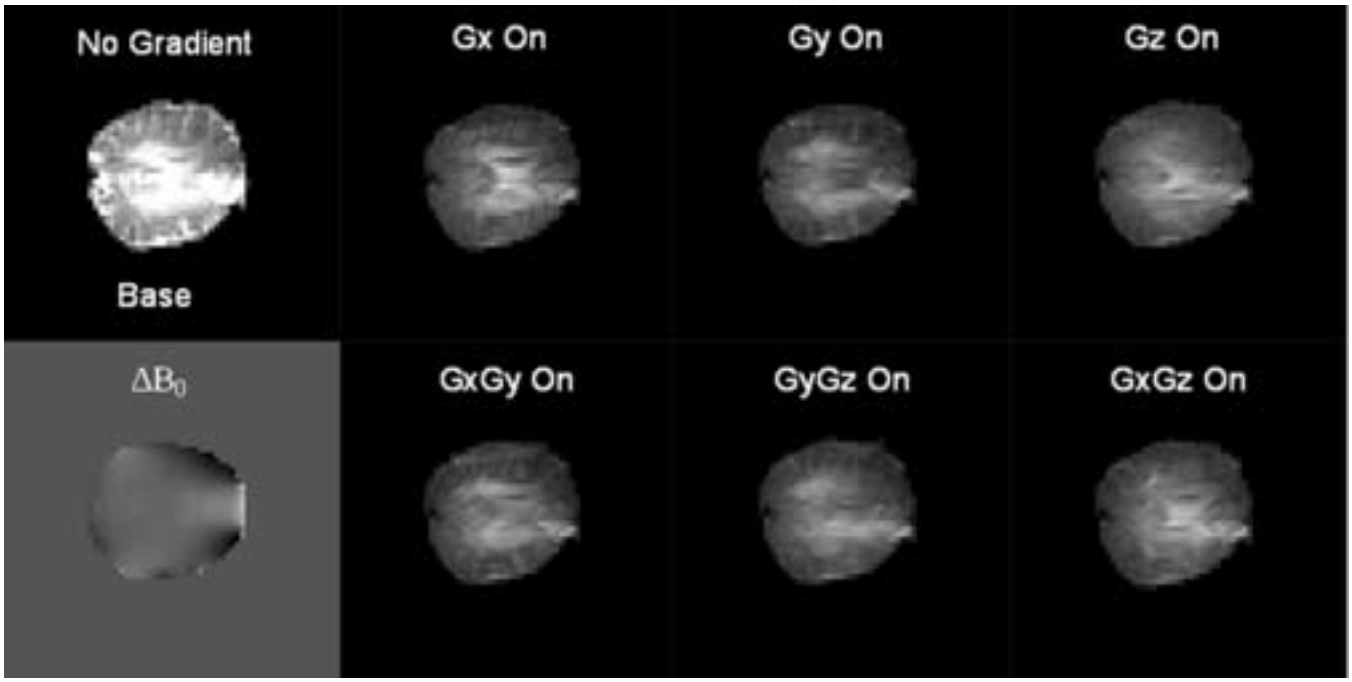
No Gradient
Gx On
Gy On
Gz On
Base
ΔB_0
GxGy On
GyGz On
GxGz On

Figure10

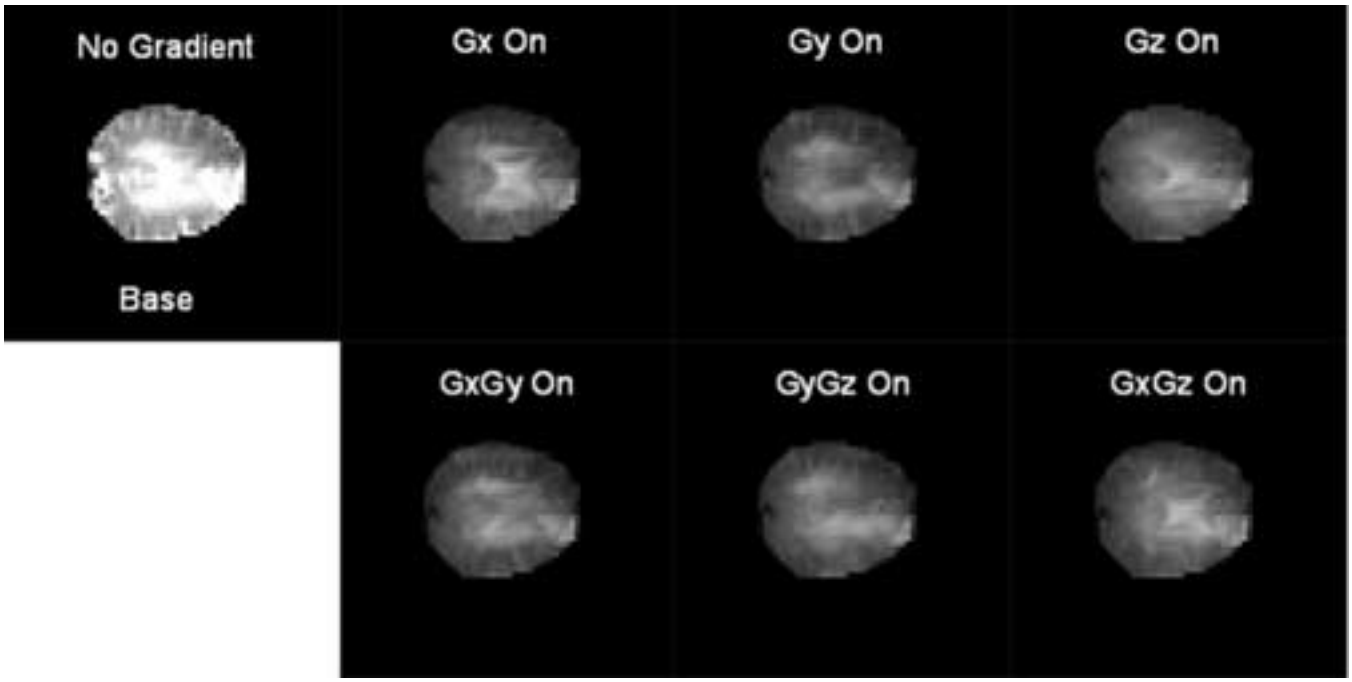

Figure11

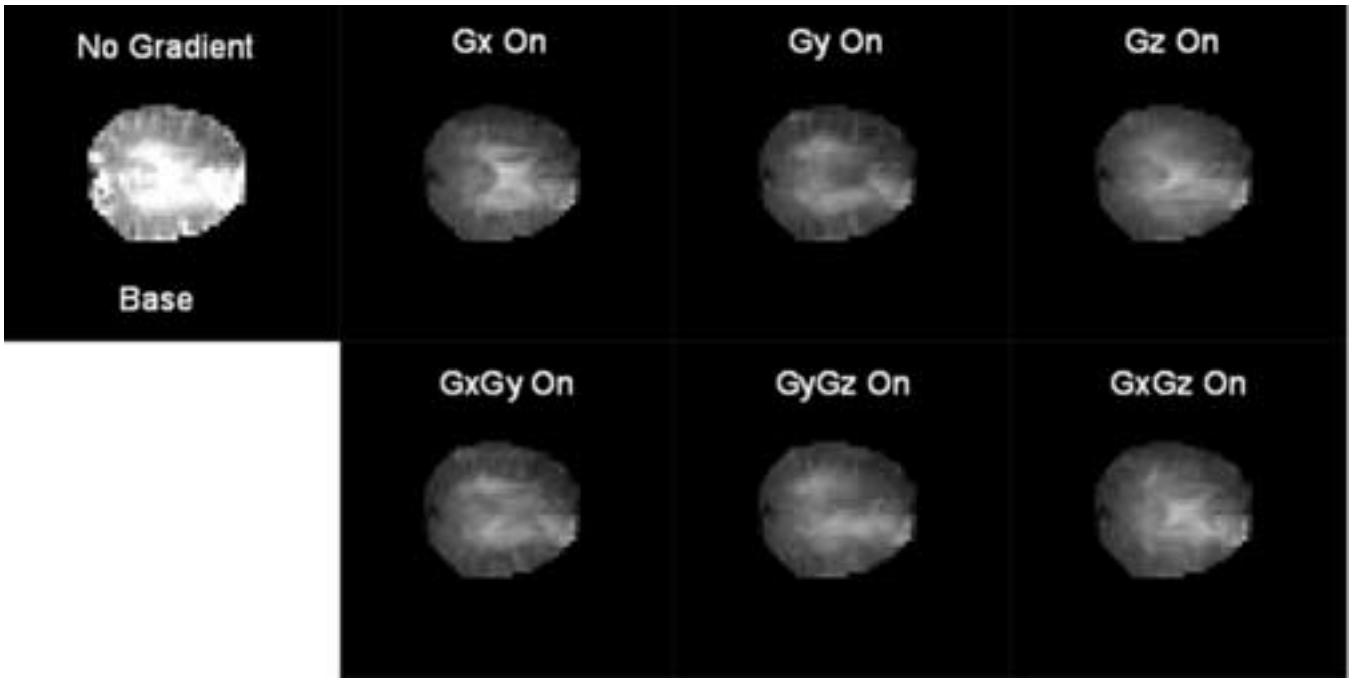

Figure12